Oil & Natural Gas Technology

DOE Award No.: DE-FE0013889

Quarterly Research Performance Progress Report (Period ending 06/30/2015)

THCM Coupled Model For Hydrate-Bearing Sediments: Data Analysis and Design of New Field Experiments (Marine and Permafrost Settings)

Project Period (10/1/2013 to 09/30/2015)

Submitted by:

Marcelo Sanchez Project PI

Texas A&M University
DUNS #: 847205572
College Station, TX
979-862-6604
msanchez@civil.tamu

Prepared for:
United States Department of Energy
National Energy Technology Laboratory
Submission date: 04/08/2015

Office of Fossil Energy

DISCLAIMER

ACCOMPLISHMENTS

The experimental study of hydrate bearing sediments has been hindered by the very low solubility of methane in water (lab testing), and inherent sampling difficulties associated with depressurization and thermal changes during core extraction. This situation has prompted more decisive developments in numerical modeling in order to advance the current understanding of hydrate bearing sediments, and to investigate/optimize production strategies and implications. The goals of this research is to addresses the complex thermo-hydro-chemo-mechanical THCM coupled phenomena in hydrate-bearing sediments, using a truly coupled numerical model that incorporates sound and proven constitutive relations, satisfies fundamental conservation principles. This tool will allow us to better analyze available data and to further enhance our understanding of hydrate bearing sediments in view of future field experiments and the development of production technology.

ACCOMPLISHED

The main accomplishments for this first period address Tasks 5, 6 and 7 of the original research plan, and include:

- Update of constitutive equations.
- Update of THCM-Hydrate.
- Numerical analyses.
- Incorporation of additional THCM-Hydrate code modifications.
- Production Optimization of Future Field Studies.

Training

The training of the two PhD students working in this project has continued during this period. Mr. Xuerui (Gary) Gai was hired at the start of the project and his activities have been related to the use of code "THCM-Hydrate"; which is the numerical tool under development in this project. In the last few months his research has focused on the mechanical modeling of Hydrate Bearing Sediments (HBS). Mr. Mehdi Teymouri was hired at the beginning of the second year of the project. His training was initially associated with gaining a better understanding on physical properties of HBS; HBS behavior and hydrate dissociation; and numerical and analytical methods in hydrates research. In the last few weeks his research has focused on sand production when producing gas from methane hydrate reservoirs. Both students have progressed positively with their coursework at their respective universities.

Literature review

The literature review (Task 2) was completed in a previous period.

Update of Update of THCM-Hydrate

The update of the constitutive laws for hydrate-bearing marine sediments and HBS in the permafrost (i.e. Task 3) was completed in a previous period.

Close-form analytical solutions

The review on the main governing evolution laws, parameters, dimensionless ratios and simplifying assumptions for HBS dissociation (i.e. Task 4) was completed in the previous period.

Numerical analyses
The numerical analyses to solve field production experiments as boundary value problems have continued in this period.

The mechanical model presented in the previous report (Sanchez and Santamaria, 2015) has been upgraded to include a more general yield function. Additional and recent experimental tests have been used to validate the model and a numerical algorithm for its implementation has been developed. The main results are presented in page 6.

In parallel progresses have been made in the modeling of methane production experiments from pressurized cores. Large scale models are also being developed to simulate real production tests. Finally, the modeling of sand production during HBS depressurization is another topic in which progress has been made in this period.

Plan - Next reporting period
We will advance analytical and numerical fronts to enhance our code to solve coupled THCM problems involving with HBS, with renewed emphasis on simulating the natural processes under *in-situ* conditions and gas production. Special emphasis will be placed on issues associated with sand production
.

Milestones for each budget period of the project are tabulated next. These milestones are selected to show progression towards project goals.

	Milestone Title Planned Date and Verification Method	Actual Completion Date	Comments
Title Related Task / Subtasks Planned Date Verification method	Complete literature review 2.0 / 2.a March 2014 Report	March 2014	Completed
Title Related Task / Subtasks Planned Date Verification method	Complete updated Constitutive Equations 2.0 / 2.b & 2.c June 2014 Report (with preliminary validation data)	July 2014	Completed
Title Related Task / Subtasks Planned Date Verification method	Validate new THCM constitutive equations 3.0 / 3.a, 3.b & 3.c September 2014 Report (with first comparisons between experimental and numerical results)	September 2014	Completed
Title Related Task / Subtasks Planned Date Verification method	Complete close-form analytical solutions 4.0 / 4.a & 4.b February 2015 Report (with analytical data)	February 2015	Completed
Title Related Task / Subtasks Planned Date Verification method	Complete numerical analyses 5.0 / 5.a, 5.b & 5.c July 2015 Report (with analytical and numerical data)	July 2015	Progressing as planned
Title Related Task / Subtasks Planned Date Verification method	Complete THCM-Hydrate code modifications 6.0 / 6.a June 2015 Report (with numerical data)	June 2015	Progressing as planned
Title Related Task / Subtasks Planned Date Verification method	Complete production optimization 7.0 / 7.a, 7.b, 7.c, 7.d & 7.e September 2015 Report (with numerical data)	September 2015	Progressing as planned

MECHANICAL MODELING OF GAS HYDRATE BEARING SEDIMENTS USING AN ELASTO-PLASTIC FRAMEWORK

1 Introduction

Methane hydrate bearing sediments (HBS) are natural soil deposits that contains ice like methane hydrates in its pore space. A proper modelling of this challenging problem will assist to study optimal methane production strategies and also to prevent the multiple hazards associated with uncontrolled hydrate dissociation and gas release from hydrate sediments. This report focuses on the mechanical modeling of HBS; which is a key component to perform realistic analyses of engineering problems involving gas hydrates. In Sanchez and Santamarina (2015) a critical state model for HBS was discussed and applied to model a set of triaxial tests carried out by Masui et al. (2005). Following the proposal by Uchida et al. (2012), the mechanical model was based on the Modified Cam-Clay (MCC) framework. Uchida et al. (2012) validated their model against published experimental data and shown that the performance of the model is very satisfactory. However, it is well known that MCC model has a number of drawbacks (especially for dealing with grained-sandy- sediments) that may limit its use in actual engineering problems. For example, the adopted ellipse shape is not very realistic for most of the sediment types, and also the MCC model overestimate significantly the failure stresses on the supercritical (dry) side (which may be relevant when studying HBS behavior).

In this study the Hierarchical Single Surface (HISS) framework proposed by Desai (1989, 2000) has been adopted in an effort to provide a more general and versatile constitutive model for HBS. Also many of the concepts suggested by Uchida et al. (2012) to deal with specific features of hydrate-bearing soils have been incorporated into this model. The proposed framework has been validated against recently published experiments involving both, synthetic and natural hydrate soils, as well as different sediments conditions (i.e., different hydrate saturations, and different hydrates morphologies) and confinements. In the following sections, the mechanical behavior of methane hydrate bearing sediment are briefly reviewed. The rationale and benefits of the adopted elasto-plastic framework are introduced afterwards, together with the application of the proposed model to reproduce the behavior of HBS tested under triaxial conditions.

2 Mechanical behavior of HBS

The mechanical behavior of methane hydrate bearing sediment is highly complex and depends on several factors. Recent studies under triaixial stress conditions have shown that synthetic methane-hydrate specimens are stronger and less compressible than hydrate-free host soils under similar conditions. The samples containing hydrates exhibit also higher shear strength, more dilation under shearing, and soften more after yielding (e.g., Masui et al., 2005; Miyazaki et al., 2011; Hyodo et al., 2013). For example, Figure 1 presents the stress-strain behavior and strain-volumetric response of natural methane hydrate samples under triaxial conditions reported by Masui (2006). It can be observed that the stiffness, peak deviatoric stress, and dilation of the samples increase with hydrate concentration. The experiments performed by Yun et al. (2007)

revealed degradation of the tangent stiffness of synthetic THF hydrate-bearing soils during shearing. In tests performed also in THF specimens it was observed that the compressibility of hydrate-soil increases with a decrease in hydrate saturation (Dai et al., 2011). In general terms, it can be concluded that the stiffness, strength and dilatancy of hydrate bearing sediments seems to increase with the increase of hydrate saturation.

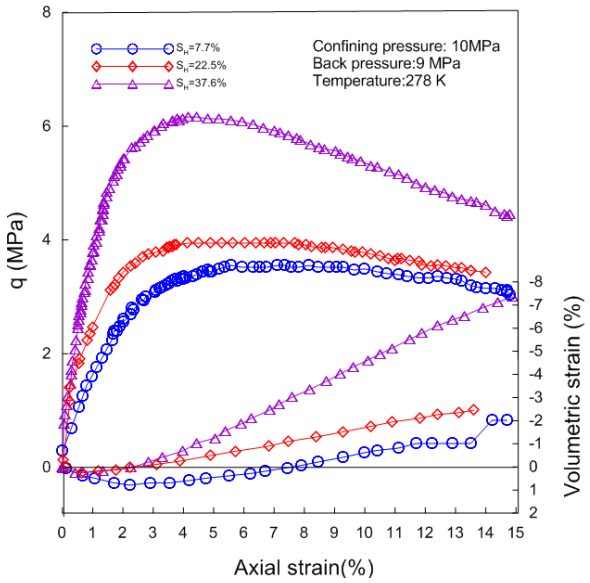

Figure 1. Tests on natural HBS samples prepared at different hydrate saturations, results in terms of stress-strain behavior and volumetric response (Masui, 2006)

The effects of hydrates on the sediment structure depend not only on the hydrate concentration (S_H), but also on the form in which the hydrates occupy the pore space. Three main kind of hydrate morphology inside the sediment structure have been recognized, namely (Figure 2): a) pore-filling, b) cementation and c) supporting matrix (Soga et al., 2006; Waite et al., 2009).

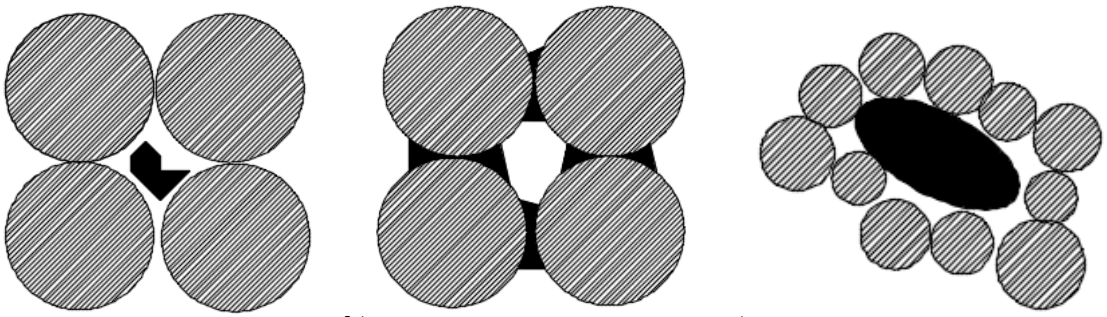

a) b) c)

Figure 2. Main types of hydrate morphology: a) pore filling; b) cementation; and c) supporting matrix.

When the hydrates habit is associated with the pore filling mode, the hydrates mainly nucleate on sediment grain boundaries and grow freely into pore spaces without bridging two or more particles together at the contact point between them. The presence of hydrates in this case can strong-

ly affects the sediment permeability and water storage capacity (e.g., Helgerud et al., 2005). Pore-filling hydrates also contribute to the mechanical stability of the granular skeleton assisting to the load-bearing framework of the sediment. If the hydrate saturation is in the order of 25%–40% (or higher) hydrate naturally turns into loadbearing hydrate (Berge et al., 1999; Yun et al., 2005, 2006). As for the second pore habit, hydrates act as a bonding material at inter-granular contacts. In this case, even a small amount of hydrate can dramatically increase the sediment shear strength and bulk stiffness by cementing adjacent grains together (e.g. Dvorkin and Uden, 2004). In the case of hydrates as supporting matrix, they are part of the solid skeleton. This type of mode is quite common in hydrates formed in fine sediments and matches the gas hydrate occurrence in Mallik 5L-38 (Dai et al., 2004). Figure 3 presents the main results of the experimental campaign performed by Masui et al. (2005) looking at the effect of hydrate pore habit on sediment mechanical behavior. It can be observed that the maximum stiffens, strength and dilatancy correspond to the case in which the hydrate is acting as a cementing material (i.e. type b, above) and the minimum ones correspond to the free-hydrate specimen. The samples related to the pore filling type exhibited an intermediate behavior.

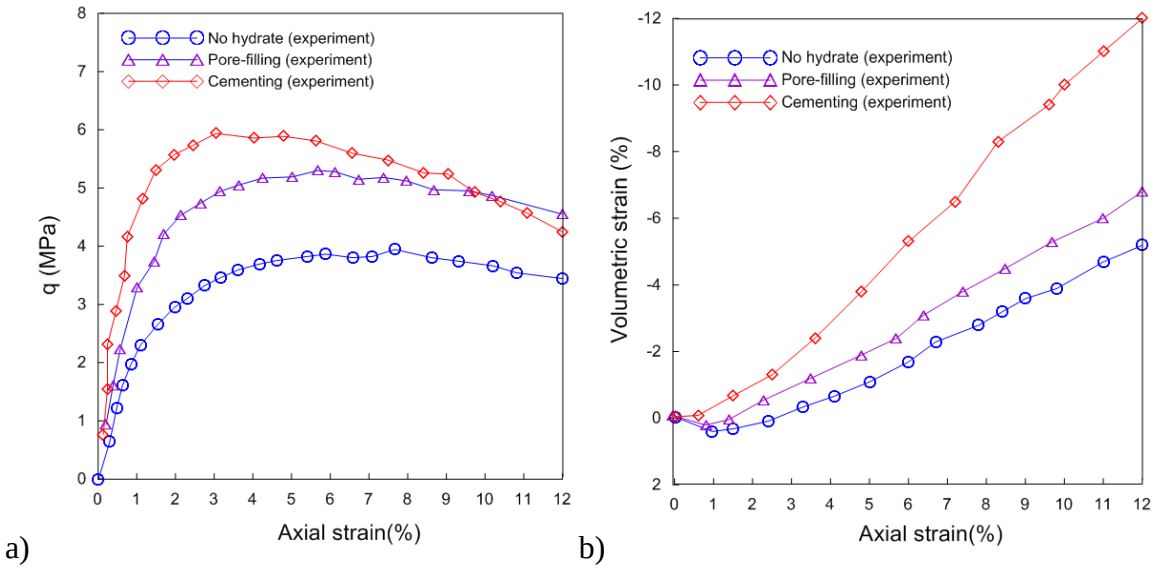

Figure 3. Experimental results of drained triaxial tests on pure Toyoura sand and hydrate samples reported by Masui et al. (2005): a) stress strain behavior, b) volumetric response.

In the following Sections the main components of the proposed elasto-plastic framework for HBS is discussed in detail, followed by the application of the model to different experiments involving hydrate soil specimens.

3 Model description

The constitutive model for HBS presented in this report is based on the Hierarchical Single Surface (HISS) framework (Desai, 1989, 2000), and add some key ingredients proposed by Uchida et al. (2012) to deal with particular features of HBS, namely: sub-loading concepts; cementing effects associated with the presence of hydrates; and bonding damage. The resulting model is

called hereafter Hierarchical Single Surface -Methane Hydrate (HISS-MH) model. Some of the model ingredients presented in a previous repot (i.e. Sanchez and Santamarina, 2015) are also discussed for the sake of the completeness.

The HISS-MH model involves a single and continuous yield surface, which can have different shapes depending on the adopted parameters. The HISS yield surface (F) is expressed as:

$$F = \frac{a}{M^2} q^2 - \gamma 3^2 p'^2 + \gamma 3^2 p'^n p_c^{2-n} \qquad (1)$$

where a and γ are constants; n is the parameter related to the transition from compressive to dilative volume change; p' and q are the mean effective and deviatoric stresses, respectively; M is the slope of critical line in the q-p' space (Figure 4); p_c is the effective pre-consolidation pressure.

An advantage of the HISS is the flexibility to adapt the shape of the yield surface to the particular conditions of the soil under investigation by modifying three parameters (a, γ and n). Figure 4 shows some of the possible yield surfaces that can be adopted with this models and the Table 1 presents the corresponding parameters. It can be seen that the MCC yield surface corresponds to a particular case of this model.

Table 1. Parameters for different yield surface

Parameters	Modified Cam-Clay model (MCC)	Cap models
a	3	3
n	1	3,5,7,9
γ	-1/9	1/9

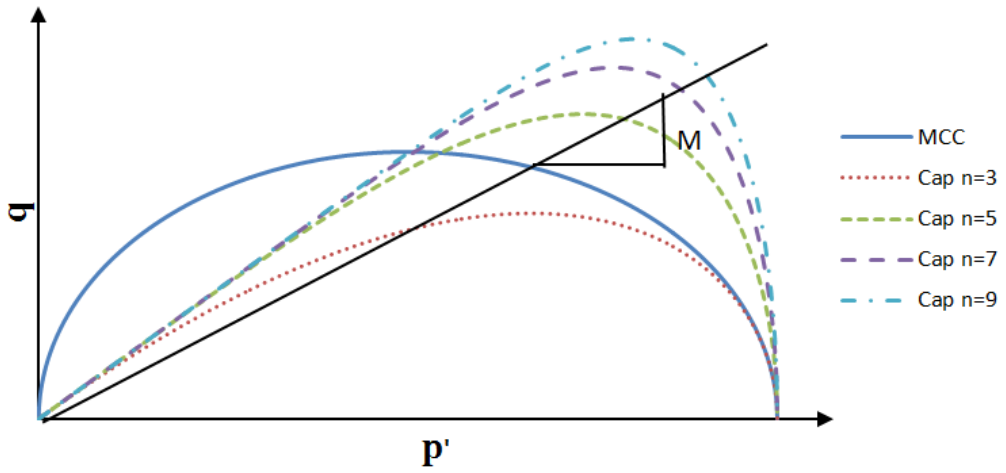

Figure 4. Different HISS yield surface options.

As in other typical soil mechanics models, the increment of the elastic volumetric strains depend directly on the increment of the mean effective stress (*p'*) through the stress-dependent elastic soil bulk modulus *K':*

$$K' = \frac{v}{\kappa} p' \tag{2}$$

where v is the specific volume (v =1+*e*, where *e* is the void ratio); and κ is the slope of the unloading/reloading line in the *e-log(p)'* space. Deviatoric elastic strains and stresses relate through the shear modulus (G_s). It is also assumed that the hardening law is isotropic and depends on the plastic volumetric strains (ε_v^p) through:

$$\frac{dp_c}{p_c} = \frac{v}{\lambda - \kappa} d\varepsilon_v^p \tag{3}$$

where λ is the slope of the normal compression line in the *e-log(p)'* space. For the sake of the simplicity, an associated flow rule is assumed in this work (i.e. F coincide with the plastic potential G), so the flow rule can be written as:

$$d\boldsymbol{\varepsilon}^p = \Lambda \frac{\partial G}{\partial \boldsymbol{\sigma}'} = \Lambda \frac{\partial F}{\partial \boldsymbol{\sigma}'} \tag{4}$$

where Λ is the plastic multiplier and $\boldsymbol{\sigma}'$ is the effective Cauchy's stress tensor.

An additional mechanism is added to the HISS model to account for the increase of strength and dilation observed in hydrate bearing sediments. This phenomenon can be associated with the cementing effects induced by the hydrates in the pore structure (Uchida et al., 2012). This mechanism will induce an isotropic expansion of the yield surface, with the related enhancement of the sediment strength (Figure 4). This effect is defined through the following evolution law:

$$p_d = \alpha \left(\chi \, S_H \right)^{\beta} \tag{5}$$

where p_d is an additional hardening parameter that controls the increase of the sediment strength associated with the presence of hydrates; α and β are constants that describe the degree of hydrate contribution to the hardening law; χ is a damage factor that varies between 1 (maximum bonding effect provided by the hydrate) and 0 (no bonding effect). It is assumed that the strength enhancement can be degraded during yielding. This effect is incorporated by defining the following evolution law for χ:

$$d\chi = -\mu \, \chi \, d\boldsymbol{\varepsilon}_q^p \tag{6}$$

where μ is a parameter that defines the rate of mechanical damage and $d\varepsilon^p{}_q$ is the plastic deviatoric strain.

The yield function of the HISS-MH model incorporating the strength enhancement effect provided by the presence of methane hydrate; which can be written as:

$$F = \frac{a}{M^2} q^2 - \gamma 3^2 p'^2 + \gamma 3^2 p'^n (p_c + p_d)^{2-n} \tag{7}$$

The model proposed above assumes that plastic strains only occur when the stresses reach the yield surface. However, in some sediments, irrecoverable strains are also observed when the stress state is inside the yield surface. It is also well-known that the conventional critical state model predicts a sharp transition between elastic and plastic states (particularly in soils that exhibit dilatancy). Sub-loading concepts are incorporated in the formulation of the constitutive equations to overcome these two limitations of the HISS model. According to Hashiguchi(1989) the sub-loading surface ratio R (with $0 < R \leq 1$) can be incorporated in the definition of the yield surface, leading to:

$$F = \frac{a}{M^2} q^2 - \gamma 3^2 p'^2 + \gamma 3^2 p'^n \left[\mathrm{R}(p_c + p_d)\right]^{2-n} \tag{8}$$

where the changes in R are defined through the following evolution law:

$$\mathrm{dR} = -\eta \ln \mathrm{R} \left| d\boldsymbol{\varepsilon}^p \right| \tag{9}$$

where $|\mathrm{d}\boldsymbol{\varepsilon}^{\mathrm{p}}|$ is the norm of the (total) plastic strain vector and η is a sub-loading parameter that controls the plastic deformations before yielding. The sub-loading surface is sketched in Figure 5. Through this plastic mechanism it is possible to model the irreversible strains generally observed when the stress sate is inside the yield surface and also to introduce a smooth transition between elastic and plastic conditions.

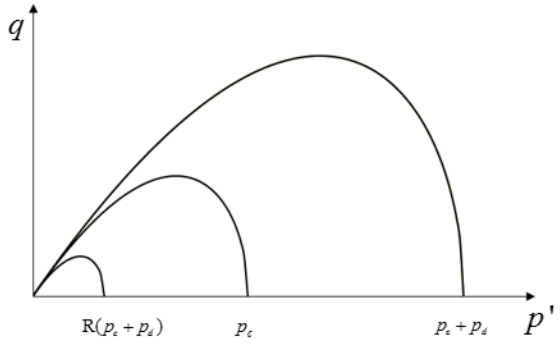

Figure 5. Yield surfaces incorporating sub-loading concepts

To ensure that the stress state remains on the yield surface during yielding the consistency condition is enforced:

$$dF = \frac{\partial \mathrm{F}}{\partial \boldsymbol{\sigma}'} : d\boldsymbol{\sigma}' + \frac{\partial F}{\partial \mathrm{p}_c} d\mathrm{p}_c + \frac{\partial \mathrm{F}}{\partial \mathrm{p}_d} d\mathrm{p}_d + \frac{\partial \mathrm{F}}{\partial \mathrm{R}} d\mathrm{R} \tag{10}$$

By substituting the flow rule Eq. (4) into the consistency condition Eq. (10), the plastic multiplier can be expressed as:

$$\Lambda = \frac{\dfrac{\partial \mathrm{F}}{\partial \boldsymbol{\sigma}'} : d\boldsymbol{\sigma}' + \dfrac{\partial \mathrm{F}}{\partial \mathrm{p}_d}\alpha\ \beta\left(\chi\ S_H\right)^{\beta-1}\chi\ dS_H}{\dfrac{\partial \mathrm{F}}{\partial \mathrm{p}_c}\dfrac{v}{\lambda-\mathrm{k}}\ p_c\dfrac{\partial \mathrm{F}}{\partial \mathrm{p}} + \dfrac{\partial \mathrm{F}}{\partial \mathrm{p}_d}\alpha\beta(-\mu)\left(\chi\ S_H\right)^{\beta}\dfrac{\partial \mathrm{F}}{\partial \mathrm{q}} + \dfrac{\partial \mathrm{F}}{\partial \mathrm{R}}(-\eta)\ln\mathrm{R}\left|\dfrac{\partial F}{\partial \boldsymbol{\sigma}'}\right|} \tag{11}$$

The effective stress-strain relationship can be obtained after multiplying the elastic constitutive matrix ($\mathbf{D}^e$) time the elastic strains; which in turns can be obtained as the difference between the total and the plastic strains, as follows:

$$d\boldsymbol{\sigma}' = \mathbf{D}^e\left(d\boldsymbol{\varepsilon} - \Lambda\frac{\partial \mathrm{F}}{\partial \boldsymbol{\sigma}'}\right) \tag{12}$$

After some algebra, the constitutive relationship can be expressed as:

$$d\boldsymbol{\sigma}' = \mathbf{D}d\boldsymbol{\varepsilon} + \mathbf{D}_{S_H}dS_H \tag{13}$$

where:

$$\mathbf{D} = \left[\mathbf{D}^e - \frac{\mathbf{D}^e\dfrac{\partial \mathrm{F}}{\partial \boldsymbol{\sigma}'}\left(\dfrac{\partial \mathrm{F}}{\partial \boldsymbol{\sigma}'}\right)^T\mathbf{D}^e}{\left(\dfrac{\partial \mathrm{F}}{\partial \boldsymbol{\sigma}'}\right)\mathbf{D}^e\dfrac{\partial \mathrm{F}}{\partial \boldsymbol{\sigma}'} + \dfrac{\partial \mathrm{F}}{\partial \mathrm{p}_c}\dfrac{v}{\lambda-\mathrm{k}}\ p_c\dfrac{\partial \mathrm{F}}{\partial \mathrm{p}} + \dfrac{\partial \mathrm{F}}{\partial \mathrm{p}_d}\alpha\beta(-\mu)\left(\chi\ S_H\right)^{\beta}\dfrac{\partial \mathrm{F}}{\partial \mathrm{q}} + \dfrac{\partial \mathrm{F}}{\partial \mathrm{R}}(-\eta)\ln\mathrm{R}\left|\dfrac{\partial F}{\partial \boldsymbol{\sigma}'}\right|}\right] \tag{14}$$

$$\mathbf{D}_{S_H} = \left[\mathbf{D}^e\frac{\dfrac{\partial \mathrm{F}}{\partial \mathrm{p}_d}\alpha\beta\left(\chi S_H\right)^{\beta-1}\chi}{\dfrac{\partial \mathrm{F}}{\partial \mathrm{p}_c}\dfrac{v}{\lambda-\mathrm{k}}\ p_c\dfrac{\partial \mathrm{F}}{\partial \mathrm{p}} + \dfrac{\partial \mathrm{F}}{\partial \mathrm{p}_d}\alpha\beta(-\mu)\left(\chi S_H\right)^{\beta}\dfrac{\partial \mathrm{F}}{\partial \mathrm{q}} + \dfrac{\partial \mathrm{F}}{\partial \mathrm{R}}(-\eta)\ln\mathrm{R}\left|\dfrac{\partial F}{\partial \boldsymbol{\sigma}'}\right|}\right] \tag{15}$$

To add the influence of temperature on the description of the sediment behavior, the Eq. (13) can be extended to consider thermomechanical effect as follows (Uchida et al., 2012):

$$d\boldsymbol{\sigma}' = \mathbf{D}d\boldsymbol{\varepsilon} + \mathbf{D}_{SH}dS_H + \frac{\partial \boldsymbol{\sigma}'}{\partial T}dT \tag{16}$$

The effective stress change due to the change in temperature is caused by the expansion of soil grains, the third term of Eq. (16) can be expressed as:

$$\frac{\partial \boldsymbol{\sigma}'}{\partial T}dT = (1-n)\beta_T K'\boldsymbol{\delta}dT = \mathbf{D}(1-n)\beta_T\frac{\boldsymbol{\delta}}{3}dT \tag{17}$$

where n is porosity, β_T is the thermal expansion coefficient of soil grains and $\boldsymbol{\delta}$ is the Kronecker's delta vector: $(1,1,1,0,0,0)^T$.

4 Model application

The performance of the model presented in Section 3 was evaluated against available experimental data involving a variety of tests, some of them published quite recently. The model was compared first against tests performed on synthetic samples prepared at a similar hydrate saturation (i.e., $S_H \sim 0.41$) but with two different type of hydrate pore habit (i.e., pore filling and cementing forms), and the tests were performed at a relatively low confinement (i.e., effective cell pressure (σ'_3) ~ 1 MPa). Then, the capability of the model to reproduce the behavior of natural samples was explored looking at the effect of hydrate saturation at relatively low confinement as well (σ'_3 ~ 1.5 MPa). Finally, the model was compared against experimental data gathered from synthetic samples prepared at different hydrate saturation (i.e. from free-hydrate samples to S_H ~ 53%), and tested at relatively high cell pressures (i.e. σ'_3 ~ 5 MPa). The main analyses are presented in the following sections.

4.1 Case study 1

Masui et al. (2005) conducted several triaxial compression tests using synthetic methane hydrate specimens. The samples containing synthetic methane hydrate were produced from two types of host specimen mixture of Toyoura sand with ice (ice-seed method) and/or with water (partial water saturation method). It can be anticipated that the ice-seed method will produce gas hydrates where the pore-filling habit is dominant, and that the partial water saturation method will form hydrates sediments where the cementing habit will be dominant. The sediments formed using the two methods were confined in a triaxial pressure vessel that replicates the pore pressure conditions equivalent to a depth of approximately 800m under the sea. Drained tests were run under a constant temperature of 278 °K and an effective confining pressure of 1.0 MPa.

Three experiments carried out by Masui et al. (2005) were selected to validate the proposed model. A triaxial compression test using pure Toyoura sand (i.e. with no hydrate) was chosen, plus two more experiments involving synthetic specimens, one of them with hydrate in pore-filling dominating habit and the other one in which the effect of the hydrate was mainly cementing. The main parameters adopted for the numerical analysis are presented in Table 2. The porosity (n) values reported by Masui et al. (2005) were between 37.7 and 42.4% and the hydrate saturation was practical identical in both tests (i.e., S_H=0.409 for the pore-filling case and S_H=0.410 for the cementing one).

Figure 5 shows the stress-strain relationship and volumetric behavior of the selected tests showing with symbols the experiments and with lines the model outputs. A marked increase in the initial stiffness and strength is observed for the pore-filling and cementing samples. It is clear that the enhancement in stiffness, strength and dilatancy is higher in cementing samples. The degradation parameter μ dependent on hydrate morphology. The critical state parameters (such as the slopes of critical state line, the normal compression line, and unloading/reloading line) are the same for both cases since they are considered independent of hydrate morphology

Table 2. Soil parameters adopted in the modeling of Toyoura sand specimens

Properties	Pure sand	Pore-filling	Cementing
M	1.47	1.47	1.47
λ	0.36	0.36	0.36
κ	0.024	0.024	0.024
p_c (MPa)	6	6	6
n	3	3	3
a	1	1	1
γ	1/9	1/9	1/9
S_H	0	0.409	0.41
α	-	15	30
β	1.6	1.6	1.6
μ	-	1.5	3.5
η	45	45	45

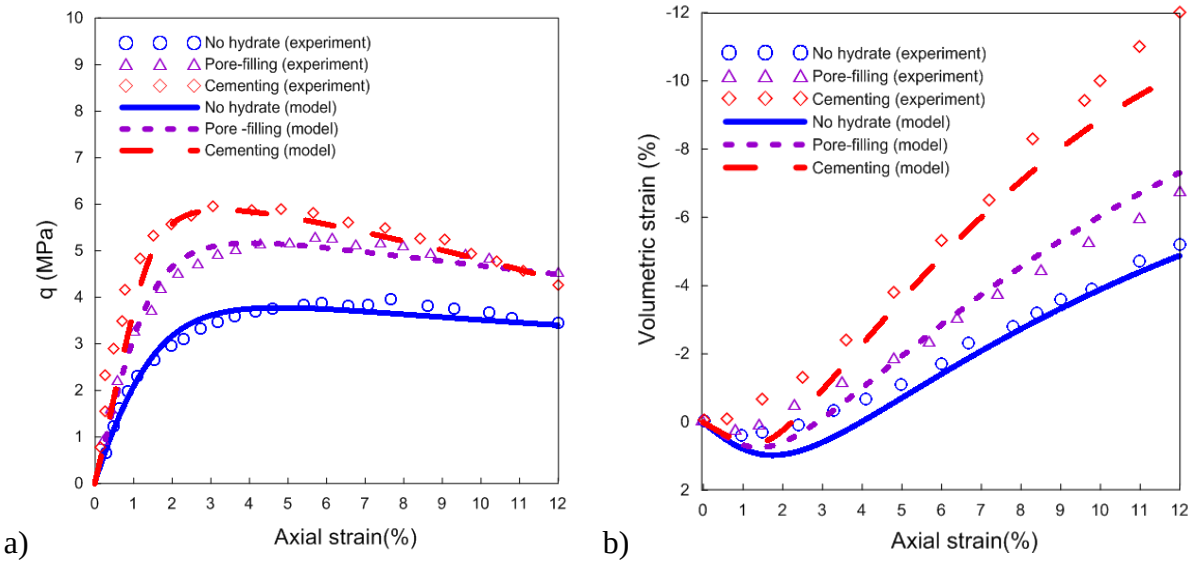

Figure 6. Modeling the drained triaxial tests on pure Toyoura sand and hydrate samples using the HISS MH model: a) stress strain behavior, b) volumetric response. Experimental data after Masui et al. (2005).

It can be observed that the model is able to capture very well the different features of HBS behavior observed in these experiments, between the pore-filling and cementing specimens, particularly in terms of peak deviatoric stresses. The model also captures well the tendencies observed in terms of soil dilatancy, with slight over-predictions.

4.2 Case study 2

The second set of tests selected to validate the proposed HISS-MH model involves natural hydrate samples studied by Yoneda et al. (2015). To investigate the mechanical behavior of natural gas-hydrate-bearing sediments several core samples were extracted from the Eastern Nankai Trough. The pressure core analysis and transfer system (PCATs) was adopted to maintain the natural sediments very close to the in-situ condition. Cores identified as Nº 7 and Nº 9, with hydrate saturation around 38% and 79%, respectively, were tested under triaxial drained condition. Table 3 presents the main soil index properties, alongside with the more relevant in-situ and testing conditions related to these samples and experiments.

Table 3. In situ conditions, soil index properties, and testing conditions

Test name	Host type	Overburden(m)	σ'_3 (MPa)	Test condition	Water Content (%)	n (%)	S_H (%)
No.7	Silty sand	279.3	1.5	CD	26.4	44.1	38
No.9	Silty sand	294.2	1.6	CD	22.7	39.4	79

Figure 7 presents the experimental stress-strain behavior and volumetric response of the natural hydrate-bearing core samples discussed above (with symbols) together with the HISS-MH model results (with lines). It is noticeable that the core Nº 9 with higher S_H exhibits a much higher peak strength and a more noticeable enhancement in stiffness and dilatancy than Core Nº 7. Since the dominant soils in both specimens are silty sands and considering that both cores were extracted from almost the same depth and around the same location, it is reasonable to assume that the difference in behavior is mainly induced by the different hydrate saturation. In order to model these different responses, it was considered the dependence of some model parameters (such as the hardening parameters p_d, α, and β) on hydrate concentration. Table 4 presents the adopted parameters. The degradation parameter μ is dependent on hydrate morphology. Considering the high concentration of hydrate in Core Nº 9, it was assumed that this specimen has a higher damage rate on shearing behavior than the sample from Core Nº 7. Also in this case the conventional critical state parameters are assumed to be the same for both cases, since they are independent of hydrate morphology/saturation.

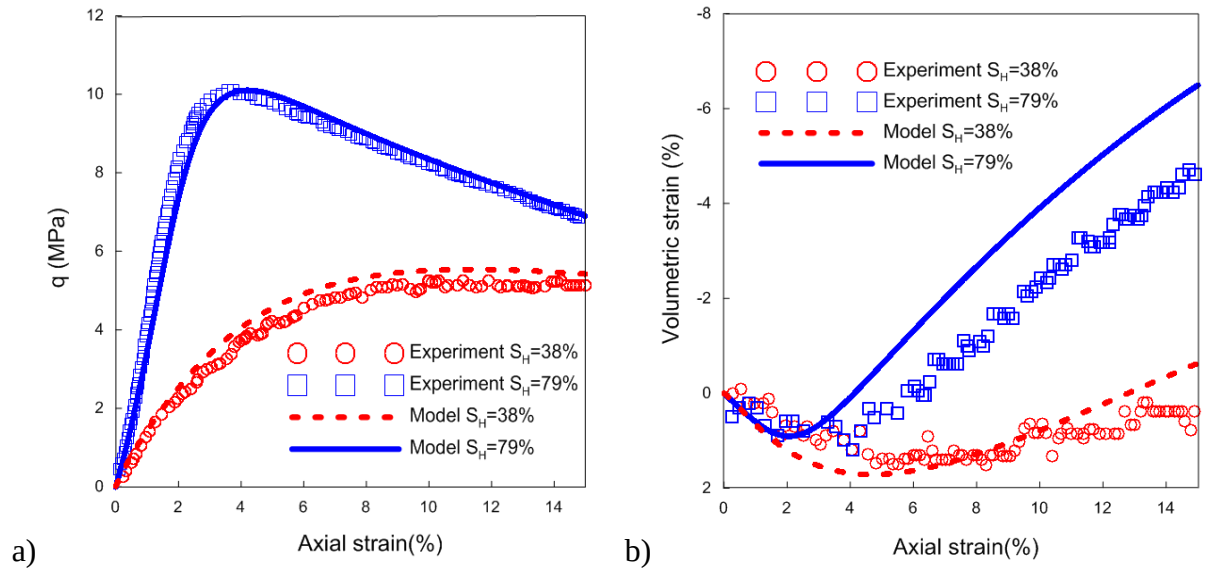

Figure 7. Modeling the drained triaxial tests on natural samples using the HISS MH model: a) stress strain behavior, b) volumetric response.

As shown in Figure 7, the HISS MH model provide enough flexibility to satisfactorily predict the mechanical behavior of two natural samples from Nankai Trough. The performance of the model is particularly good for Core Nº 7, with a good simulation of the stress-stain behavior and dilatancy reported by Yoneda (2015). However, the model over predicts the dilation of core Nº 9. This is a topic that perhaps need more research.

Table 4. Soil parameters adopted in the modeling of HBS specimens

Properties	Core 7	Core 9
M	1.37	1.37
λ	0.16	0.16
κ	0.008	0.008
p_c (MPa)	12	12
n	1	1
a	3	3
γ	-1/9	-1/9
S_H	0.36	0.79
α	12	32
β	1.6	1.0
μ	1.5	2.0
η	15	15

4.3 Case Study 3

The third and final set of experimental data studied in this research corresponds to tests reported by Hyodo et al. (2013). They carried out a series of triaxial compression tests on synthetic methane hydrate-bearing soil in order to study the mechanical behavior of HBS. The global porosity

of all the samples were quite similar (n ~ 40%). The following S_H were investigated: 0, 24.2; 35.1, and 53.1 %. The effective confining pressure for all the tests was 5 MPa and the temperature during the experiments was around 5 ◦C. The main test conditions in this experimental study are summarized in Table 5.

Table 5. Test conditions for triaxial compression tests

Effective confining pressure (MPa)	Temperature (C)	Porosity (%)	Degree of hydrate saturation (%)
5	5	39.4	0
5	5	39.6	24.2
5	5	39.2	35.1
5	5	40.1	53.1

Figure 8 shows the responses of specimens with different hydrate saturations in terms of deviatoric stress, axial and volumetric strains, for samples that where isotropically consolidated first and subjected to shearing afterwards. It is observed that most of specimens shown a dominant compressive volume change and strain hardening behavior at this (relatively high) level of confining pressure. Only the sample with the higher hydrate saturation (i.e., S_H=53.1%) presents a notorious dilative behavior. Also in these tests, a marked increase in the initial stiffness and shear strength is observed with the increase of hydrate saturation of the samples.

As in the previous case studies, the hydrate dependent parameters were adjusted accordingly to fit the available experimental observations discussed above. Table 6 presents the parameters used in the numerical simulations. In summary, it can be said that the model was able to match quite well the stress-strain curves for four of the five tests under study, with only a slight over prediction of the devitoric stress for the highest hydrate saturation (i.e., S_H=53.1%). In terms of volumetric strains, the largest difference between model results and experiments was less than 2% for all the tests analyzed.

Table 6: Soil parameters adopted in the modeling of HBS specimens

Properties	Test 1	Test 2	Test 3	Test 4
M	1.50	1.53	1.68	1.72
λ	0.16	0.16	0.16	0.16
κ	0.004	0.004	0.004	0.004
$p_c(MPa)$	7.0	7.0	7.0	7.0
n	5	5	5	7
a	3	3	3	3
γ	1/9	1/9	1/9	1/9
S_H	0	0.242	0.351	0.531
α	-	22	22	22
β	-	1.6	1.6	1.6
μ	-	1.5	1.5	0.5
η	55	55	55	55

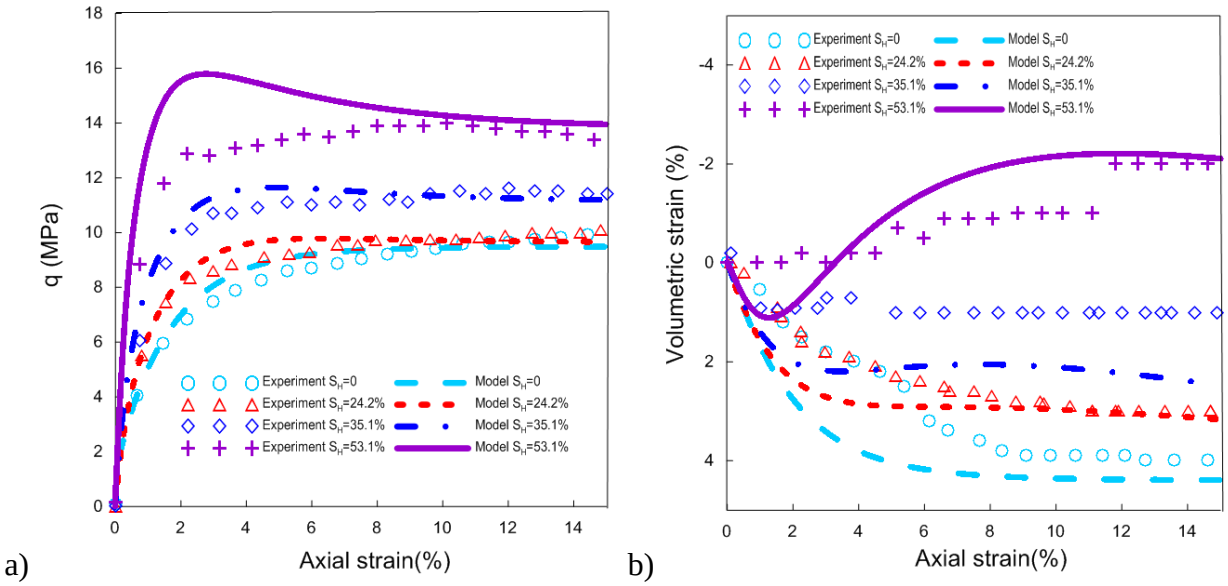

Figure 8. Modeling the drained triaxial tests on synthetic samples using the HISS MH model: a) stress strain behavior, b) volumetric response

5 CONCLUSIONS

In this research a constitutive model for hydrate bearing soil was presented. The core of the proposed model includes: a HISS critical state framework, sub-loading concepts for modeling the plastic strains generally observed inside the yield surface and a hydrate enhancement factor to account for the cementing effects provided by the presence of hydrates in sediments. The model was developed in the framework of elasto-plastic theory for strain hardening/softening soils, incorporating bonding and damage effects. The formal full mathematical framework was presented and discussed in detail.

The model performance against published experimental data was also investigated using a variety of available tests, some of them published quite recently. The tests involving different hydrate saturations (i.e., from free-hydrate samples up to S_H=79%), different types of hydrate pore habits (i.e., pore filling and cementing morphologies) and different range of confinement conditions (i.e. σ'_3 from 1 MPa up to 5 MPa). It was observed that the model was able to reproduce quite satisfactorily the enhanced stiffness and strength induced by the presence of methane hydrate in the sediment pore space, as well as the soil dilatancy observed in the triaxial experiments. The model was also capable of capturing the difference in the mechanical response associated with different S_H values and also with the type of hydrate morphology. This model also performs well under different ranges of confining pressure. Under low confining conditions, it was observed that the hydrate sediment behaved mainly as a strain softening material, with a marked dilatant behavior. While at higher confinements, the HBS samples tended to act mainly as a strain hard-

ening material, with contraction under shearing loads, this response was particularly true for samples with not very high hydrate saturation (i.e. $S_H < 35\%$). A small drawback of the proposed model is that in some cases it tends to over predicts the HBS dilation (i.e., simulation of the Yuneda et al., 2015 test with $S_H=79\%$) or the HBS shear strength (i.e., simulation of Hyodo et al., 2013 test with $S_H=53{,}1\%$). In spite of these minor issues, it can be considered that the global response of the HISS-MH model was very satisfactory under the variety of HBS types test conditions considered in this study.

References

Berge, L.I., K.A. Jacobsen, and A. Solstad, *Measured acoustic wave velocities of R11 (CCl3F) hydrate samples with and without sand as a function of hydrate concentration.* Journal of Geophysical Research: Solid Earth (1978–2012), 1999. 104(B7): p. 15415-15424.

Collett, T.S., *Energy resource potential of natural gas hydrates.* AAPG bulletin, 2002. 86(11): p. 1971-1992.

Dai, J., H. Xu, F. Snyder, and N. Dutta, *Detection and estimation of gas hydrates using rock physics and seismic inversion: Examples from the northern deepwater Gulf of Mexico.* The Leading Edge, 2004. 23(1): p. 60-66.

Dai, S., C. Lee, and J.C. Santamarina, *Formation history and physical properties of sediments from the Mount Elbert Gas hydrate stratigraphic test well, Alaska North Slope.* Marine and Petroleum Geology, 2011. 28(2): p. 427-438.

Desai, C., *Letter to editor single surface yield and potential function plasticity models: A review.* Computers and Geotechnics, 1989. 7(4): p. 319-333.

Desai, C.S., *Mechanics of materials and interfaces: The disturbed state concept*2000: CRC press.

Dvorkin, J. and R. Uden, *Seismic wave attenuation in a methane hydrate reservoir.* The Leading Edge, 2004. 23(8): p. 730-732.

Helgerud, M., J. Dvorkin, A. Nur, A. Sakai, and T. Collett, *Elastic-wave velocity in marine sediments with gas hydrates: Effective medium modeling.* Geophysical Research Letters, 1999. 26(13): p. 2021-2024.

Hyodo, M., J. Yoneda, N. Yoshimoto, and Y. Nakata, *Mechanical and dissociation properties of methane hydrate-bearing sand in deep seabed.* Soils and foundations, 2013. 53(2): p. 299-314.

Kvenvolden, K.A., *Potential effects of gas hydrate on human welfare.* Proceedings of the National Academy of Sciences, 1999. 96(7): p. 3420-3426.

Masui, A., H. Haneda, Y. Ogata, and K. Aoki. *Effects of methane hydrate formation on shear strength of synthetic methane hydrate sediments*. in *The Fifteenth International Offshore and Polar Engineering Conference*. 2005. International Society of Offshore and Polar Engineers.

Masui, A., H. Haneda, Y. Ogata, and K. Aoki. *Triaxial compression test on submarine sediment containing methane hydrate in deep sea off the coast of Japan* (in Japanese), paper presented at the 41st Annual Conference, Jpn. Geotech. Soc., Kagoshima, 2006, Japan, 12–14 July

Miyazaki, K., A. Masui, Y. Sakamoto, K. Aoki, N. Tenma, and T. Yamaguchi, *Triaxial compressive properties of artificial methane-hydrate-bearing sediment.* Journal of Geophysical Research: Solid Earth (1978–2012), 2011. 116(B6).

Miyazaki, K., N. Tenma, K. Aoki, and T. Yamaguchi, *A nonlinear elastic model for triaxial compressive properties of artificial methane-hydrate-bearing sediment samples.* Energies, 2012. 5(10): p. 4057-4075.

Pinkert, S. and J. Grozic, *Prediction of the mechanical response of hydrate-bearing sands.* Journal of Geophysical Research: Solid Earth, 2014. 119(6): p. 4695-4707.

Sanchez and Santamaria (2015). "*THCM Coupled Model For Hydrate-Bearing Sediments: Data Analysis and Design of New Field Experiments (Marine and Permafrost Settings*)". DOE Quarterly Research Performance Progress Report (Period ending 03/31/2015).

Soga, K., S. Lee, M. Ng, and A. Klar, *Characterisation and engineering properties of methane hydrate soils.* Characterisation and engineering properties of natural soils, 2006: p. 2591-2642.

Uchida, S., K. Soga, and K. Yamamoto, *Critical state soil constitutive model for methane hydrate soil.* Journal of Geophysical Research: Solid Earth (1978–2012), 2012. 117(B3).

Waite, W.F., J.C. Santamarina, D.D. Cortes, B. Dugan, D. Espinoza, J. Germaine, J. Jang, J. Jung, T.J. Kneafsey, and H. Shin, *Physical properties of hydrate-bearing sediments.* Reviews of Geophysics, 2009. 47(4).

Yoneda, J., A. Masui, Y. Konno, Y. Jin, K. Egawa, M. Kida, T. Ito, J. Nagao, and N. Tenma, *Mechanical properties of hydrate-bearing turbidite reservoir in the first gas production test site of the Eastern Nankai Trough.* Marine and Petroleum Geology, 2015.

Yun, T., F. Francisca, J. Santamarina, and C. Ruppel, *Compressional and shear wave velocities in uncemented sediment containing gas hydrate.* Geophysical Research Letters, 2005. 32(10).

Yun, T.S., J.C. Santamarina, and C. Ruppel, *Mechanical properties of sand, silt, and clay containing tetrahydrofuran hydrate.* Journal of Geophysical Research: Solid Earth (1978–2012), 2007. 112(B4).

PRODUCTS

Publications – Presentations:

- A conference paper has been accepted for the 'XV Pan-American Conference on Soil Mechanics and Geotechnical Engineering, to be held in Buenos Aires, 15th to 18th November 2015 Title: "Mechanical Modeling of Gas Hydrate Bearing Sediments Using an Elasto-Plastic Framework". Authors: Xuerui Gai, and M. Sanchez.
- A Panel Session on Gas Hydrate Bearing Sediments was organized in the framework of "1st Symposium on Energy Geotechnics" hold in Barcelona, Spain, between 2nd and 4th June 2015. Dr. Sanchez was the moderator of the panel and Dr. Santamaria one of panelists.
- An extended abstract entitled 'Modeling the behavior of gas hydrate bearing sediments' was submitted and the related presentation was delivered at the "1st Symposium on Energy Geotechnics" hold in Barcelona, Spain, between 2nd and 4th June 2015. Authors: Marcelo Sánchez, J. Carlos Santamarina, Ajay Shastri, and Xuerui Gai. Presented by Marcelo Sanchez.
- A session on "Hydrate bearing sediments: characterization, modeling and implications on geohazard and gas production", has been accepted for the forthcoming AGU Fall meeting 2015, San Francisco, 14th to 18th December 2015. Marcelo Sanchez is one of the session conveners.
- A journal paper has been prepared. Title: "Mechanical behavior of frozen soils: experimental investigational and constitutive modeling". Authors: Ajay Shastri, Marcelo Sánchez, Moo Y. Lee, and Thomas Dewers.
- A journal paper has been prepared. Title: "Mechanical Modeling of Gas Hydrate Bearing Sediments Using an Elasto-Plastic Framework". Authors: Xuerui Gai, and M. Sanchez.

Website: Publications (for academic purposes only) and key presentations are included in: http://engineering.tamu.edu/civil/people/msanchez

Technologies or techniques: None at this point.

Inventions, patent applications, and/or licenses: None at this point.

Other products: None at this point.

PARTICIPANTS

Research Team: The current team is shown next.

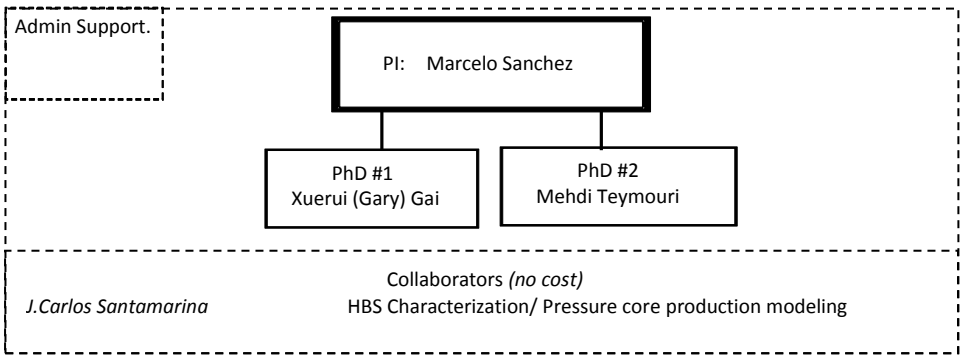

IMPACT

- We can already highlight the computational platform extensively validated in a wide range of coupled thermo-hydro-chemo-mechanical coupled problems (CB_Hydrate).

CHANGES/PROBLEMS:

None so far.

SPECIAL REPORTING REQUIREMENTS:

Nothing to report

BUDGETARY INFORMATION:

Grant No.DE-FE0013889										EXHIBIT 2- COST PLAN/STATUS							
TEES Project 32525-C3870 CE																	
COST PLAN/STATUS																	
				Budget Period 1									Budget Period 2				
	Q1		Q2		Q3		Q4		Q1		Q2		Q3		Q4	
	Enter date range		Enter date range		Enter date range		Enter date range		Enter date range		Enter date range		Enter date range		Enter date range	
Baseline Reporting Quarter	10/1/13- 12/31/13		01/01/14-03/31/14		04/01/14-06/30/14		07/01/14-9/30/14		10/1/14-12/31/2014		01/01/15-03/31/15		04/01/15-06/30/15		07/01/15-9/30/15	
		Cumulative		Cumulative		Cumulative		Cumulative		Cumulative		Cumulative		Cumulative		Cumulative
	Q1	Total	Q2	Total	Q3	Total	Q4	Total	Q1	Total	Q2	Total	Q3	Total	Q4	Total
Baseline Cost Plan	$ 40,500.00	$ 40,500.00	$ 40,500.00	$ 81,000.00	$ 40,500.00	$ 121,500.00	$ 92,180.00	$ 213,680.00	$ 27,600.00	$ 241,280.00	$ 27,600.00	$ 268,880.00	$ 27,600.00	$ 296,480.00	$ 92,080.00	$ 388,560.00
Federal Share	$ 40,500.00	$ 40,500.00	$ 40,500.00	$ 81,000.00	$ 40,500.00	$ 121,500.00	$ 92,180.00	$ 213,680.00	$ 27,600.00	$ 241,280.00	$ 27,600.00	$ 268,880.00	$ 27,600.00	$ 296,480.00	$ 92,080.00	$ 388,560.00
Non-Federal Share	$ 11,223.00	$ 11,223.00	$ 11,223.00	$ 22,446.00	$ 11,223.00	$ 33,669.00	$ 11,223.00	$ 44,892.00	$ 11,223.00	$ 56,115.00	$ 11,223.00	$ 67,338.00	$ 11,223.00	$ 78,561.00		
Total Planned	$ 51,723.00	$ 51,723.00	$ 51,723.00	$ 103,446.00	$ 51,723.00	$ 155,169.00	$ 103,403.00	$ 258,572.00	$ 38,823.00	$ 297,395.00	$ 38,823.00	$ 336,218.00	$ 49,023.00	$ 385,241.00		
Actual Incurred Costs	$ 5,301.83	$ 5,301.83	$ 13,764.34	$ 19,066.17	$ 33,827.48	$ 52,893.65	$ 51,567.77	$ 104,461.42	$ 80,352.17	$ 184,813.59	$ 24,626.18	$ 209,439.77	$ 19,260.19	$ 228,699.96		
Federal Share	$ 3,335.02	$ 3,335.02	$ 9,848.68	$ 13,183.70	$ 10,170.37	$ 23,354.07	$ 58,205.62	$ 81,559.69	$ 92,208.79	$ 173,768.48	$ 31,359.66	$ 205,128.14	$ 19,260.19	$ 224,388.33		
Non-Federal Share	$ 5,182.96	$ 5,182.96	$ 20,751.77	$ 25,934.73	$ 20,743.19	$ 46,677.92	$ 29,262.19	$ 75,940.11	$ -	$ 75,940.11	$ -	$ 75,940.11	$ 8,833.66	$ 84,773.77		
Total Incurred costs	$ 8,517.98	$ 8,517.98	$ 30,600.45	$ 39,118.43	$ 30,913.56	$ 70,031.99	$ 87,467.81	$ 157,499.80	$ 92,208.79	$ 249,708.59	$ 31,359.66	$ 281,068.25	$ 28,093.85	$ 309,162.10		
Varience	$ 43,205.02	$ 43,205.02	$ 21,122.55	$ 64,327.57	$ 20,809.44	$ 85,137.01	$ 15,935.19	$ 101,072.20	$ (53,385.79)	$ 47,686.41	$ 38,823.00	$ 55,149.75	$ 20,929.15	$ 76,078.90		
Federal Share	$ (1,966.81)	$ (1,966.81)	$ (3,915.66)	$ (5,882.47)	$ (23,657.11)	$ (29,539.58)	$ 6,637.85	$ (22,901.73)	$ 11,856.62	$ (11,045.11)	$ 6,733.48	$ (4,311.63)	$ -	$ (4,311.63)		
Non-Federal Share	$ 6,040.04	$ 6,040.04	$ (9,528.77)	$ (3,488.73)	$ (9,520.19)	$ (13,008.92)	$ (40,485.19)	$ (53,494.11)	$ 11,223.00	$ (42,271.11)	$ 6,733.48	$ (35,537.63)	$ 2,389.34	$ (33,148.29)		
Total Varience	$ 4,073.23	$ 4,073.23	$ (13,444.43)	$ (9,371.20)	$ (33,177.30)	$ (42,548.50)	$ (33,847.34)	$ (76,395.84)	$ 23,079.62	$ (53,316.22)	$ 13,466.96	$ (39,849.26)	$ 2,389.34	$ (37,459.92)		

National Energy Technology Laboratory

626 Cochrans Mill Road
P.O. Box 10940
Pittsburgh, PA 15236-0940

3610 Collins Ferry Road
P.O. Box 880
Morgantown, WV 26507-0880

13131 Dairy Ashford Road, Suite 225
Sugar Land, TX 77478

1450 Queen Avenue SW
Albany, OR 97321-2198

Arctic Energy Office
420 L Street, Suite 305
Anchorage, AK 99501

Visit the NETL website at:
www.netl.doe.gov

Customer Service Line:
1-800-553-7681